

# Evidence for a truncated accretion disc in the low-luminosity Seyfert galaxy, NGC 7213?

A. P. Lobban,<sup>1\*</sup> J. N. Reeves,<sup>1</sup> D. Porquet,<sup>2</sup> V. Braito,<sup>3</sup> A. Markowitz,<sup>4</sup> L. Miller<sup>5</sup> and T. J. Turner<sup>6</sup>

<sup>1</sup>*Astrophysics Group, School of Physical and Geographical Sciences, Keele University, Keele, Staffordshire ST5 8EH*

<sup>2</sup>*Observatoire astronomique de Strasbourg, Université de Strasbourg, CNRS, UMR 7550, 11 rue de l'Université, F-67000 Strasbourg, France*

<sup>3</sup>*Department of Physics and Astronomy, University of Leicester, University Road, Leicester LE1 7RH*

<sup>4</sup>*Center for Astrophysics and Space Sciences, University of California, San Diego, M.C. 0424, La Jolla, CA 92093-0424, USA*

<sup>5</sup>*Department of Physics, University of Oxford, Denys Wilkinson Building, Keble Road, Oxford OX1 3RH*

<sup>6</sup>*Department of Physics, University of Maryland Baltimore County, Baltimore, MD 21250 and Astrophysics Science Division, NASA/GSFC, Greenbelt, MD 20771, USA*

Accepted 2010 June 4. Received 2010 May 28; in original form 2010 February 9

## ABSTRACT

We present the broad-band 0.6–150 keV *Suzaku* and *Swift* BAT spectra of the low-luminosity Seyfert galaxy, NGC 7213. The time-averaged continuum emission is well fitted by a single power law of photon index  $\Gamma = 1.75$ , and from consideration of the *Fermi* flux limit we constrain the high-energy cut-off to be  $350 \text{ keV} < E_{\text{cut}} < 25 \text{ MeV}$ . Line emission from both near-neutral iron  $\text{K}\alpha$  at 6.39 keV and highly ionized iron, from Fe xxv and Fe xxvi, is strongly detected in the *Suzaku* spectrum, further confirming the results of previous observations with *Chandra* and *XMM-Newton*. We find the centroid energies for the emission from Fe xxv and Fe xxvi to be 6.60 and 6.95 keV respectively, with the latter appearing to be resolved in the *Suzaku* spectrum. From modelling, we show that the Fe xxv and Fe xxvi emission can result from a highly photoionized plasma, with a column density of  $N_{\text{H}} \sim 3 \times 10^{23} \text{ cm}^{-2}$ . A Compton reflection component, e.g. originating from an optically thick accretion disc or a Compton-thick torus, appears either very weak or absent in this active galactic nucleus (AGN), subtending  $< 1 \text{ sr}$  to the X-ray source, consistent with previous findings. Indeed, the absence of Compton reflection from either neutral or ionized material coupled with the lack of any relativistic Fe K signatures in the spectrum suggests that an inner, optically thick accretion disc is absent in this source. Instead, the accretion disc could be truncated with the inner regions perhaps replaced by a Compton-thin radiatively inefficient accretion flow (RIAF). Thus, the Fe xxv and Fe xxvi emission could both originate in ionized material perhaps at the transition region between the hot, inner flow and the cold, truncated accretion disc on the order of  $10^3$ – $10^4$  gravitational radii from the black hole. The origin for the unresolved neutral Fe  $\text{K}\alpha$  emission is then likely to be further out, perhaps originating in the optical broad-line region or a Compton-thin pc-scale torus.

**Key words:** accretion, accretion discs – atomic processes – galaxies: active – galaxies: Seyfert – X-rays: galaxies.

## 1 INTRODUCTION

NGC 7213 is a nearby low-luminosity active galactic nucleus (AGN;  $z = 0.005839$ ), often classified as an intermediate between a Seyfert 1 and a low-ionization nuclear emission-line region (LINER) galaxy due to its optical spectrum (Filippenko & Halpern 1984). Its X-ray spectral properties also appear to lie between those of weak AGN (e.g. M81) and ‘classical’ higher-luminosity broad-

line Seyferts. The ultraviolet (UV) flux measured by Wu, Boggess & Gull (1983) was higher than would be expected from an extrapolation of the optical flux, indicating that NGC 7213 may have a big blue bump (BBB), although weak compared to most Seyferts. This object has a high black hole mass of about  $10^8 M_{\odot}$  as estimated from the stellar velocity dispersion (Nelson & Whittle 1995; Woo & Urry 2002) and a low bolometric luminosity ( $L_{\text{bol}}$ ) of about  $9 \times 10^{42} \text{ erg s}^{-1}$  (Starling et al. 2005).

NGC 7213 has a very low accretion rate of only 0.07 per cent  $L_{\text{Edd}}$ , a value which is intermediate between those usually found

\*E-mail: apl@astro.keele.ac.uk

in local type 1 Seyfert galaxies (e.g. Padovani & Rafanelli 1988; Wandel 1999; Page 2001) and LINERs (e.g. Ho 1999). Interestingly, this is much less than the predicted 2 per cent  $L_{\text{Edd}}$  ‘critical’ rate whereby the high/soft state in black hole X-ray binaries can be observed (Maccarone 2003). Furthermore, this object exhibits another interesting characteristic since it is part of a class of Seyfert galaxies which have radio properties that are intermediate between those of radio-loud and radio-quiet active galaxies (e.g. Blank, Harnett & Jones 2005 and reference therein). It is therefore conceivable that NGC 7213 is an analogue of the Galactic low/hard state sources.

Simultaneous *XMM-Newton* (new EPIC-pn exposure  $\sim 30$  ks) and *BeppoSAX* observations in 2001 May revealed further peculiar characteristics of NGC 7213. The low signal-to-noise ratio (S/N) reflection grating spectrometer (RGS) spectrum showed the presence of several weak emission features with no absorption lines (Starling et al. 2005) contrary to what is usually found in Seyfert type 1 galaxies. Moreover, the emission lines appeared to be the signature of a collisionally ionized thermal plasma ( $k_{\text{B}}T \sim 0.18$  keV), while in Seyfert galaxies, only emission and/or absorption lines from a photoionized warm absorber/emitter have before been observed (e.g. NGC 3783, Kaspi et al. 2001; NGC 4151, Schurch & Warwick 2002; NGC 1068, Kinkhabwala et al. 2002; Brinkman et al. 2002; Mrk 3, Pounds & Page 2005). Such emission lines from collisionally ionized thermal plasma have, however, been observed in the soft X-ray spectra of LINERs, such as M81 (Page et al. 2003). Interestingly, no significant Compton reflection was observed in these simultaneous *XMM-Newton* and *BeppoSAX* observations (reflection component:  $R = \Omega/2\pi < 0.2$ , where a value  $R = 1$  corresponds to reflection off material subtending  $2\pi$  sr; Bianchi et al. 2003), though the presence of a significant Fe K complex could be explained by three narrow emission lines: neutral iron at around 6.40 keV with an EW of  $\sim 80$  eV, Fe xxv at around 6.66 keV and Fe xxvi at about 6.94 keV (see also Starling et al. 2005).

Bianchi et al. (2003) deduced from the absence of the reflection component that the neutral iron  $K\alpha$  emission line is most likely produced in a Compton-thin torus or the broad-line region (BLR). Indeed, according to Matt, Perola & Pirlo (1991) and George & Fabian (1991), a line with an EW of  $\sim 80$  eV would require a reflection component of about  $R \sim 0.6$ , a larger value than that found for this object ( $R < 0.2$ ). Furthermore, Bianchi et al. (2008) reported the data analysis of a long *Chandra* HETG observation of NGC 7213 finding that the neutral iron  $K\alpha$  line is resolved with a full width at half-maximum (FWHM) value of  $2400_{-600}^{+1100}$  km s $^{-1}$ , fully consistent with the  $H\alpha$  linewidth ( $2640_{-90}^{+110}$  km s $^{-1}$ ) measured with the European Southern Observatory New Technology Telescope (ESO NTT). They therefore inferred that the neutral Fe K line seen in this object originates in the Compton-thin BLR explaining the lack of evidence for Compton reflection. They also confirmed the presence of two ionized iron lines at  $\sim 6.72$  and  $\sim 6.99$  keV which they associate most probably with the resonance transition of the Fe xxv triplet and the  $Ly\alpha$  transition of Fe xxvi, respectively. Comparing the line energies found with their rest-frame values, a blueshift of about 900 km s $^{-1}$  is inferred. If the dominant line at  $\sim 6.72$  keV is indeed the resonance line of the Fe xxv triplet, then this means that the line may be associated with a collisionally ionized thermal plasma (Bautista & Kallman 2000; Porquet & Dubau 2000).

Here, we report on a 90 ks *Suzaku* (Mitsuda et al. 2007) observation of NGC 7213. The overall goal is to understand accretion in an AGN at low rates compared to Eddington, through a high S/N, broad-band observation of this source. Specifically, the objectives are to parametrize the iron line complex with an analysis of the X-ray Imaging Spectrometer (XIS) spectra in order to constrain the

individual properties of the lines before considering the complete broad-band spectra from 0.6 to 150 keV with a combined analysis of the *Suzaku* XIS and Hard X-ray Detector (HXD) data with that from the time-averaged *Swift* BAT 22-month survey (see Section 3). The aims are to obtain better constraints on the origin of both the iron line complex and any observed soft excess whilst simultaneously testing for the presence (or absence) of a Compton reflection component (see Section 4).

## 2 SUZAKU ANALYSIS AND DATA REDUCTION

### 2.1 *Suzaku* analysis

NGC 7213 was observed by *Suzaku* on 2006 October 22 with a total net exposure of 90 ks. In this paper we discuss data taken from the four XIS (Koyama et al. 2007) CCDs and the PIN diodes of the HXD (Takahashi et al. 2007).

Event files from version 2.0.6.13 of the *Suzaku* pipeline processing were used. All event files were screened within XSELECT to exclude data taken within the South Atlantic Anomaly (SAA) as well as excluding data with an Earth elevation angle (ELV)  $< 5^\circ$ . Data taken with Earth day-time elevation angles (DYE\_ELV) less than  $20^\circ$  were also excluded. A cut-off rigidity (COR) criteria of  $>6$  GeV/c for the XIS was applied. Only good events with grades 0, 2, 3, 4 and 6 were used, while hot and flickering pixels were removed from the XIS images using the CLEANIS script. Time intervals affected by telemetry saturation were also removed.

Subsequently, source spectra from the XIS CCDs were extracted from circular regions of 2.3 arcmin radius centred on the source, in the on-axis XIS nominal pointing position. Background spectra were extracted from 2.3 arcmin circles offset from the source region, avoiding the calibration sources on the corners of the CCD chips. XIS response files (RMFs) and ancillary response files (ARFs) were generated using the XISRMFGEN and XISSIMARFGEN FTOOLS, respectively, including correction for the hydrocarbon contamination on the optical blocking filter (Ishisaki et al. 2007). A net XIS source exposure of 90.7 ks was obtained for each of the four XIS chips. The three front-illuminated XIS chips (XIS 0, 2, 3; hereafter XIS-FI) are predominantly used in this paper as they have the greatest sensitivity at iron K. These chips were found to produce consistent spectra within the statistical errors, so the spectra and responses were combined to maximize S/N. The net source count rate for the three XIS combined was  $1.585 \pm 0.002$  count s $^{-1}$  per XIS, with the background rate only 0.7 per cent of the source rate. This count rate corresponds to an observed flux of  $2.46 \times 10^{-11}$  erg cm $^{-2}$  s $^{-1}$  and a luminosity of  $1.85 \times 10^{42}$  erg s $^{-1}$  over the 2–10 keV range. The XIS source spectrum was binned at the half width at half-maximum (HWHM) resolution of the detector due to the high photon statistics. This enabled the use of  $\chi^2$  minimization as there were  $>50$  counts per resolution bin. Errors are quoted to 90 per cent confidence for 1 parameter (i.e.  $\Delta\chi^2 = 2.7$ ) unless otherwise stated.

### 2.2 HXD reduction

As NGC 7213 is below the detection threshold of the HXD GSO, we used data from the HXD PIN only, where this object is detected at the  $13\sigma$  level relative to the background. The source spectrum was extracted from the cleaned HXD PIN events files and processed with the screening criteria described above. The HXD PIN instrumental background spectrum was generated from a ‘tuned’ time-dependent model provided by the HXD instrument team (Fukazawa et al. 2009). Both the source and background spectra were made with

identical good time intervals (GTIs) and the source exposure was corrected for detector deadtime (which is  $\approx 6.7$  per cent). A detailed description of the PIN detector deadtime is given in Kokubun et al. (2007). The net exposure time of the PIN source spectrum was 84.3 ks after deadtime correction. Note that the background spectral model was generated with 10 times the actual background count rate in order to minimize the photon noise on the background; this has been accounted for by increasing the effective exposure time of the background spectra by a factor of  $\times 10$ . The HXD PIN response file dated 2008/01/29 (epoch 3) for the XIS nominal position was used for these spectral fits.

In addition, a spectrum of the cosmic X-ray background (CXB) (Boldt 1987; Gruber et al. 1999) was also simulated with the HXD PIN. The form of the CXB was taken as  $9.0 \times 10^{-9} (E/3 \text{ keV})^{-0.29} \exp(-E/40 \text{ keV}) \text{ erg cm}^{-2} \text{ s}^{-1} \text{ sr}^{-1} \text{ keV}^{-1}$ . When normalized to the field of view of the HXD PIN instrument, the effective flux of the CXB component is  $8.49 \times 10^{-12} \text{ erg cm}^{-2} \text{ s}^{-1}$  in the 15–50 keV band corresponding to a count rate of  $\sim 0.017 \text{ counts s}^{-1}$ . The net flux of NGC 7213 measured by the HXD over the same band is  $3.58 \times 10^{-11} \text{ erg cm}^{-2} \text{ s}^{-1}$ , i.e. the CXB component represents 24 per cent of the net source flux measured by the HXD PIN. Note that there may be some uncertainty in the absolute flux level of the CXB component measured between missions; for instance, Churazov, Sunyaev & Revnivtsev (2007) find the CXB normalization from *INTEGRAL* to be about 10 per cent higher than measured by Gruber et al. (1999) from the HEAO-1 data. However, a factor of  $\pm 10$  per cent uncertainty in the CXB normalization would result in a  $\pm 2.4$  per cent uncertainty in the HXD flux for NGC 7213, which is well within the statistical uncertainty of the HXD PIN observations. After background subtraction (including both the instrumental and CXB components), the resulting net PIN source count rate from 15–50 keV was  $0.062 \pm 0.002 \text{ count s}^{-1}$  corresponding to a 15–50 keV flux of  $3.58 \times 10^{-11} \text{ erg cm}^{-2} \text{ s}^{-1}$ . Note that the total background count rate was  $\sim 0.350 \text{ count s}^{-1}$  (15–50 keV) with a typical  $1\sigma$  systematic uncertainty of  $\pm 1.3$  per cent.

We used 0.6–10 keV data in both the XIS–FI and XIS–BI spectra. We ignored the 1.7–1.9 keV band in the co-added FI spectrum and the BI spectrum due to uncertainties in calibration associated with the instrumental Si K edge. In all fits, we included a constant multiplicative factor to account for relative instrument normalizations. We allowed the relative XIS–BI/XIS–FI normalization to vary, but best-fitting values were always within 1 per cent of each other.

A visual analysis of the light curves was undertaken to determine whether any detailed timing analysis was necessary. It can be seen from Fig. 1 that the amplitude of the XIS–FI light curve varies only by a factor of  $\sim 0.1$  throughout the entire observation indicating little intrinsic variability below 10 keV. From Fig. 2, it can be seen that the HXD PIN light curve, too, shows little evidence of any substantial variability in the hard X-ray band. Therefore, due to the lack of any strong evidence of short-time-scale spectral variability, we proceed to consider the time-averaged spectrum (Section 3).

### 3 SPECTRAL ANALYSIS

The XSPEC v11.3 software package (Arnaud 1996) was used for the spectral analysis of the background-subtracted spectrum. In all fits, we included the Galactic column density ( $N_{\text{H}}^{\text{Gal}} = 1.1 \times 10^{20} \text{ cm}^{-2}$ , obtained from the FTOOL NH using the compilations of Dickey & Lockman 1990 and Kalberla et al. 2005) and used the cross-sections for X-ray absorption by the interstellar medium from Morrison & McCammon (1983). Note that all fit parameters are given in the rest

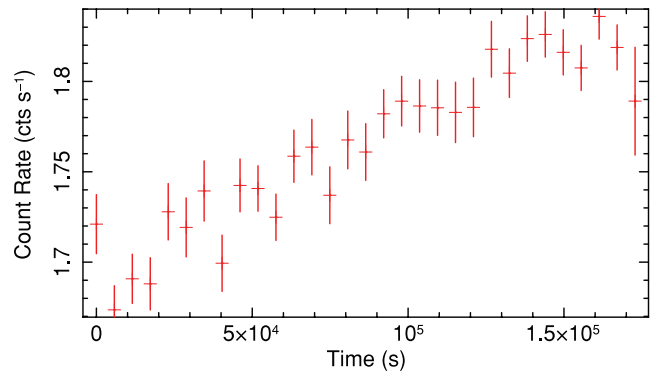


**Figure 1.** XIS–FI background-subtracted light curve of NGC 7213 from 0.5 to 10 keV in 5760 s orbital bins.

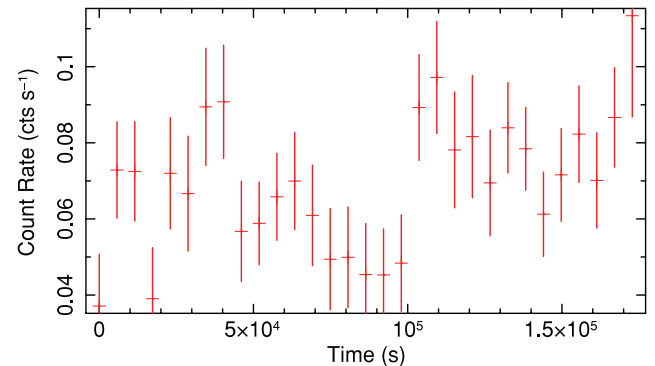


**Figure 2.** Net background-subtracted HXD PIN light curve of NGC 7213 from 15 to 50 keV in 5760 s orbital bins.

frame of the galaxy, assuming a distance of 25 Mpc to NGC 7213 (Mould et al. 2000). Abundances are those of Anders & Grevesse (1989) unless otherwise stated.

The cross-normalization between the HXD PIN and XIS detectors was accounted for by the addition of a fixed constant component at a value of 1.16 for the XIS nominal pointing position, a value derived using *Suzaku* observations of the Crab (Ishida, Suzuki & Someya 2007<sup>1</sup>).

#### 3.1 The Fe K line profile

The X-ray spectrum was initially analysed in the 0.6–50 keV band using both the XIS–FI and HXD PIN data. A power law with Galactic absorption of column density  $N_{\text{H}} = 1.1 \times 10^{20} \text{ cm}^{-2}$  was fitted to the data revealing a slight soft excess at energies  $< 1 \text{ keV}$  as shown in Fig. 3. The XIS 1 data were included in this fit to check for consistency. For clarity, the HXD data were binned to  $10\sigma$  per spectral bin relative to the background. The hard X-ray data are seen to extrapolate quite well to the XIS data with very few residuals in excess of the power-law continuum indicating little or no reflection component ( $R \sim 0.2$ ; see Section 3.2). Line emission is clearly present with a strong but seemingly relatively narrow Fe K $\alpha$  line at  $\sim 6.4 \text{ keV}$ . As the XIS 1 has a much lower S/N ratio at higher energies above 2 keV, these data were initially excluded from the Fe K line analysis leaving the XIS–FI to be analysed from 2.5 to 10 keV. The HXD data were also initially excluded as the lack of Compton reflection suggested that the Fe K emission lines could be

<sup>1</sup> ftp://legacy.gsfc.nasa.gov/suzaku/doc/xrt/suzakumemo-2007-11.pdf

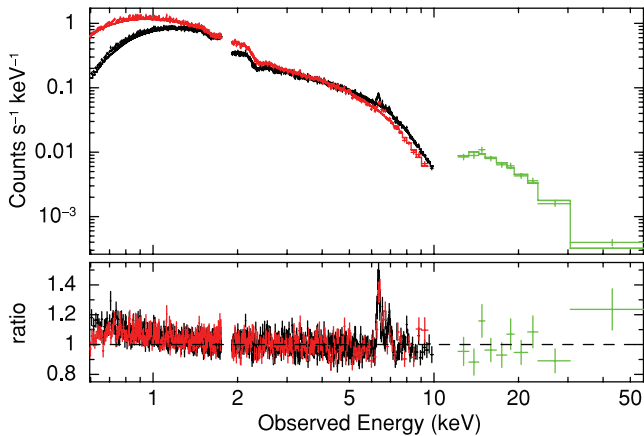


**Figure 3.** The *Suzaku* spectra of NGC 7213 (in the observed frame) showing the XIS-FI (black), XIS-BI (red) and HXD PIN (green). An absorbed (Galactic column density) power law has been fit to the broad-band spectrum. A significant positive residual is observed in the Fe K complex energy range, as well as a weak excess in the  $<1$  keV energy range.

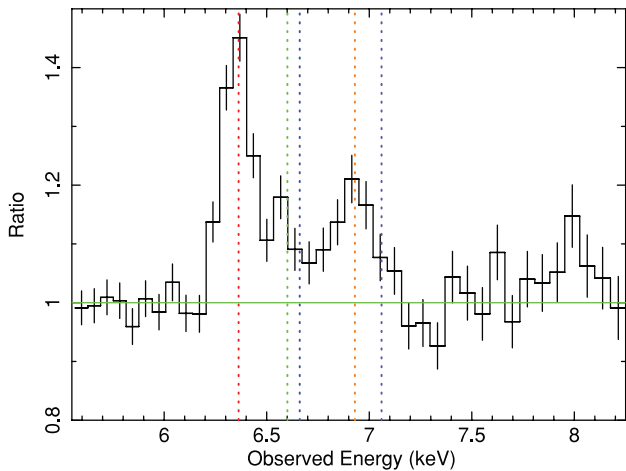


**Figure 4.** A plot of the ratio of the residuals for the XIS-FI data of the Fe line complex compared to the power-law continuum. The spectra are binned relative to the half-width at half-maximum of the detector resolution. The vertical dotted lines show the expected line energies of, from left to right, Fe  $K\alpha$ , Fe xxv forbidden, Fe xxv  $1s-2p$  resonance, Fe xxvi  $1s-2p$  Ly $\alpha$  and Fe  $K\beta$  in the observed frame.

modelled independently. The HXD and XIS 1 data are re-included in the broad-band fits in Section 3.2.

A simple power-law model of  $\Gamma = 1.75 \pm 0.02$  with Galactic absorption evidently resulted in a poor fit ( $\chi^2/\text{d.o.f.} = 739/316$ ) highlighted by a low null hypothesis probability of  $6.67 \times 10^{-36}$ . A plot of the ratio of the residuals with respect to the power-law continuum from 5.0 to 8.5 keV (Fig. 4) clearly shows X-ray line emission which requires modelling; the most apparent being the Fe  $K\alpha$  line from near-neutral material at  $6.39 \pm 0.01$  keV with an intrinsic width of  $\sigma < 4.30 \times 10^{-2}$  keV, equivalent width of  $\text{EW} = 83.1^{+11.0}_{-10.7}$  eV and an observed flux of  $F_{K\alpha} = 2.18^{+0.28}_{-0.29} \times 10^{-5}$  photon  $\text{cm}^{-2} \text{s}^{-1}$ . Adding this line improves the fit significantly with a value of  $\Delta\chi^2 = 316.8$  for three parameters of interest. However, even upon modelling the strong Fe  $K\alpha$  line at 6.39 keV, the fit remains unacceptable (null probability =  $3.70 \times 10^{-5}$ ) with further residuals still present between 6.5–7.0 keV indicating K-shell emission from ionized Fe.

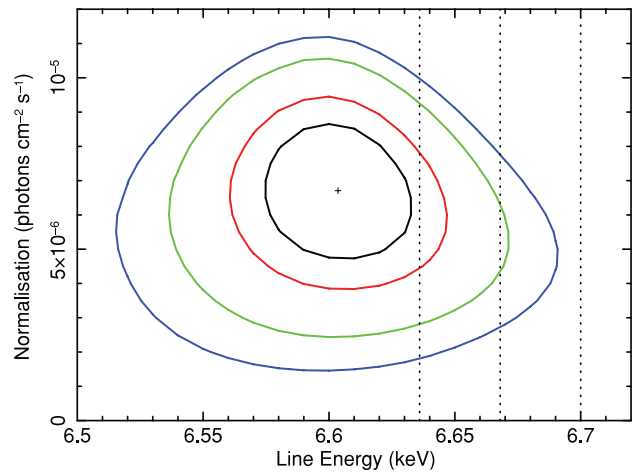


**Figure 5.** A two-dimensional contour plot between line energy and normalization of the 6.60 keV line at the 68 per cent, 90 per cent, 99 per cent and 99.9 per cent confidence intervals (inner to outer contours, respectively) for two parameters of interest. The vertical dashed lines show the rest energies of the forbidden, intercombination and resonance transitions of the Fe xxv triplet at 6.637, 6.668 and 6.700 keV, respectively.

Further Gaussian lines were added to fit other prominent emission lines starting with the  $1s-2p$  doublet from hydrogen-like iron (Fe xxvi) at  $6.95 \pm 0.03$  keV which corresponds to a value of  $\Delta\chi^2 = 57.1$  for an additional three parameters of interest. Unlike the 6.39 keV line, this line appears to be resolved compared to the detector resolution with an intrinsic width of  $\sigma = 0.10^{+0.05}_{-0.04}$  keV (FWHM  $\sim 10$  000  $\text{km s}^{-1}$ ), an equivalent width of  $\text{EW} = 62.3^{+16.0}_{-14.2}$  eV and an observed flux of  $F_{\text{line}} = 1.40^{+0.36}_{-0.32} \times 10^{-5}$  photon  $\text{cm}^{-2} \text{s}^{-1}$ . A third narrow component at a line energy of  $6.60 \pm 0.03$  keV was also modelled, improving the fit by a factor of  $\Delta\chi^2 = 32.8$  for a further three parameters of interest. A line energy versus line flux contour plot (Fig. 5) shows that this line energy can be rejected at the 99.9 per cent confidence level (for two interesting parameters) as being associated with the resonance line of helium-like iron (Fe xxv) at 6.700 keV ( $\Delta\chi^2 \sim 14$ ) and is just acceptable (rejected at only 90 per cent confidence) as the forbidden line at 6.637 keV (also see Section 3.3.2).<sup>2</sup> The fact that this indicates that the line at 6.60 keV is more consistent with the forbidden transition of Fe xxv is an interesting discovery since the resonance line is expected to dominate over the forbidden line in a collisionally ionized plasma (Porquet & Dubau 2000; Bautista & Kallman 2000). Further discussion regarding the origin of this emission can be found in Section 4.2.

A weak, narrow component appeared to remain in the residuals at a line energy of  $8.00^{+0.10}_{-0.14}$  keV with an intrinsic width of  $\sigma < 0.28$  keV. However, the detection is more marginal; adding this extra line component only improves the fit by  $\Delta\chi^2 = 10.0$  for three parameters. This putative line could possibly be associated with the  $1s-3p$  transitions of Fe xxv or Fe xxvi (corresponding to rest energies of  $\sim 7.88$  and  $\sim 8.25$  keV, respectively) or alternatively, it could be due to the  $1s-2p$  transition of H-like nickel (corresponding to a rest energy of  $\sim 8.10$  keV). Finally, no neutral  $K\beta$  emission was apparent but was still modelled for consistency at a fixed line energy of 7.06 keV, with an intrinsic width,  $\sigma$ , tied to that of the corresponding  $K\alpha$  line. The upper limit on the flux of  $F_{K\beta} < 0.67 \times$

<sup>2</sup> An analysis of the spectrum produced by the XIS Fe-55 calibration source, which produces emission lines from Mn  $K\alpha$  and Mn  $K\beta$ , shows that the absolute XIS energy scale is accurate to within  $\pm 10$  eV.

**Table 1.** Spectral parameters to the *Suzaku* XIS data in the Fe K band.

Model component	Fit parameter	Value	$\chi^2/\text{d.o.f.}$	$\Delta\chi^2$
1. Power-law continuum <sup>a</sup>	$\Gamma$	$1.75 \pm 0.02$		
	Normalization	$6.25^{+0.02}_{-0.06}$		
	$F_{2.5-10\text{keV}}$	$2.18 \times 10^{-11}$		
2. Galactic absorption <sup>b</sup>	$N_{\text{H}}$	$1.10 \times 10^{20}$	739/316	
3. Fe K $\alpha$ line <sup>c</sup>	$E_{\text{line}}$	$6.39 \pm 0.01$	422/313	316.8
	$\sigma$	$<4.30 \times 10^{-2}$		
	EW	$83.1^{+11.0}_{-10.7}$		
	FWHM	$<4600$		
	Line flux	$2.18^{+0.28}_{-0.29}$		
4. H-like line <sup>c</sup>	$E_{\text{line}}$	$6.95 \pm 0.03$	365/310	57.1
	$\sigma$	$0.10^{+0.05}_{-0.04}$		
	EW	$62.3^{+16.0}_{-14.2}$		
	FWHM	$10000^{+5000}_{-4000}$		
	Line flux	$1.40^{+0.36}_{-0.32}$		
5. 6.60 keV line <sup>c</sup>	$E_{\text{line}}$	$6.60 \pm 0.03$	332/307	32.8
	$\sigma$	$<0.30$		
	EW	$24.4 \pm 8.0$		
	FWHM	$<32000$		
	Line flux	$0.67 \pm 0.22$		
6. 8.00 keV line <sup>c</sup>	$E_{\text{line}}$	$8.00^{+0.10}_{-0.14}$	322/304	10.0
	$\sigma$	$<0.28$		
	EW	$45.9^{+33.5}_{-27.7}$		
	FWHM	$<25000$		
	Line flux	$0.78^{+0.57}_{-0.47}$		
7. Fe K $\beta$ line <sup>c</sup>	$E_{\text{line}}$	7.06	322/304	0.5
	$\sigma$	$<4.30 \times 10^{-2}$		
	EW	$<29.3$		
	FWHM	$<4600$		
	Line flux	$<0.67$		
8. Fit statistics <sup>d</sup>	$\chi^2/\text{d.o.f.}$	322/304		
	Null probability	0.36		

<sup>a</sup>  $\Gamma$ , photon index; normalization in units  $\times 10^{-3}$  photon  $\text{cm}^{-2} \text{s}^{-1}$ ;  $F_{2.5-10\text{keV}}$ , absorbed continuum flux from 2.5 to 10 keV in units of  $\text{erg cm}^{-2} \text{s}^{-1}$ .

<sup>b</sup> Local Galactic absorption (at  $z = 0$ ), units  $\text{cm}^{-2}$ .

<sup>c</sup>  $E_{\text{line}}$ , line energy in units keV;  $\sigma$ ,  $1\sigma$  linewidth in units keV; EW, equivalent width in units eV; FWHM, full width at half maximum in units  $\text{km s}^{-1}$ ; Line Flux in units  $\times 10^{-5}$  photon  $\text{cm}^{-2} \text{s}^{-1}$ . <sup>d</sup> Reduced chi-squared ( $\chi^2/\text{d.o.f.}$ ) and null hypothesis probability for the spectral fit.

$10^{-5}$  photon  $\text{cm}^{-2} \text{s}^{-1}$  then provided an upper limit on the K $\beta$ /K $\alpha$  flux ratio of 0.35. A value of  $\Delta\chi^2 = 0.5$  revealed that the K $\beta$  line is consistent with the fit to the data but in this instance is not required. Hereafter, we include the K $\beta$  line fixed at 13 per cent of the K $\alpha$  flux in all subsequent fits to remain consistent with the theoretical flux ratio for neutral iron (Kaastra & Mewe 1993).

We did also attempt to model the neutral Fe K $\alpha$  emission with a DISKLINE component (Fabian et al. 1989) to test for the presence of any broad, relativistic emission from the inner regions of the accretion disc. We fixed the width of the original Gaussian at 6.39 keV to be narrow ( $\sigma = 10$  eV) in order to model emission from distant material and introduced a DISKLINE component to the model with the centroid energy fixed at 6.39 keV and the emissivity index fixed at a standard value of  $q = 3$ . We also fixed the inner and outer radii of the emission at 6 and  $400 R_g$  from the black hole, respectively (where  $6 R_g$  corresponds to the innermost stable orbit for a Schwarzschild black hole) and the inclination angle of the source at  $\theta = 30^\circ$ . Upon fitting, this returned a value for the flux of the line of  $F_{\text{diskline}} < 7.64 \times 10^{-6}$  photon  $\text{cm}^{-2} \text{s}^{-1}$  which corresponds to a 90 per cent upper limit on the equivalent width of the line of EW  $< 26.8$  eV. This tight constraint appears to exclude the presence

of any Fe K emission from the inner accretion disc. We note that no other significant emission or absorption lines are found in the Fe K band. The values of all of the final parameters and fit statistics are noted in Table 1.

### 3.2 The broad-band spectrum

The first stage of the broad-band spectral analysis was to model the spectra above 10 keV by including the *Suzaku* HXD PIN data. To check for consistency, the 22-month time-averaged *Swift* BAT spectra (14–150 keV) were also included (Tueller et al. 2010). This provided an extension of the spectrum far beyond the high energy limit of the HXD PIN. We restricted the energy range of the HXD from 15 to 50 keV and applied a constant multiplicative factor of 1.16 to account for the cross-normalization at the XIS nominal pointing position. The constant in front of the BAT data was allowed to be free as the 14–150 keV flux over the 22-month period (2004/12/15–2006/10/27) may have varied (time-averaged flux  $F_{14-150} = 5.31 \times 10^{-11}$   $\text{erg cm}^{-2} \text{s}^{-1}$ ). This provided a cross-normalization factor of  $0.75 \pm 0.11$  for the BAT compared to the *Suzaku* XIS. The power-law component was replaced by an

exponential cut-off power law and we note that no cut-off energy is required in these data. We constrain the 90 per cent lower limit on  $E_{\text{cut}} > 350$  keV. A simultaneous *XMM-Newton* and *BeppoSAX* PDS observation published by Bianchi et al. (2004) required a high-energy cut-off with a value of  $E_{\text{cut}} = 90^{+50}_{-20}$  keV. However, fixing the cut-off energy at 90 keV in our *Suzaku*+BAT spectrum results in a worse fit with  $\Delta\chi^2 = 35$  supportive of the notion that the cut-off appears to be at significantly higher energy in these data.

The residuals in the hard X-ray regime show very little excess flux above 10 keV when modelled with a power law indicating a lack of a Compton reflection component. To test for this, we included the *PEXRAV* model (Magdziarz & Zdziarski 1995) which is an additive component incorporating the reflected continuum from a neutral slab. We tied the photon index of the power law incident upon the reflector to that of the power-law continuum and fixed the elemental abundances to Solar (Anders & Grevesse 1989). We also fixed the cosine of the inclination angle of the source to 0.87 and tied the folding energy to the cut-off energy of the power law at  $\sim 1000$  keV, consistent with no cut-off as above. The inclusion of the *PEXRAV* component resulted in a reflection scaling factor value of  $R = 0.18^{+0.23}_{-0.14}$ , consistent with the *XMM-Newton/BeppoSAX* analysis of Bianchi et al. (2004) who find  $R < 0.19$ . The inclusion of this component corresponds to  $\Delta\chi^2 \approx 5.0$  suggesting that this component is only marginally required. This resulted in a fit statistic  $\chi^2/\text{d.o.f.} = 486/446$ , acceptable with a null hypothesis probability of 0.10.

The next step was to model the entire broad-band spectra by including the XIS data below 2.5 keV. As the S/N decreases at lower energies, the spectra were only included down to 0.6 keV for each XIS. The data were also ignored from 1.7 to 1.9 keV so as not to include the silicon absorption edge due to the detectors. The inclusion of these data resulted in a slightly worse fit with a null probability of  $2.98 \times 10^{-3}$ . Residuals were observed at energies  $< 2$  keV hinting at the presence of a weak soft excess (e.g. Fig. 3). Upon closer inspection of these residuals, it was noted that the XIS 1 (BI) detector data slightly diverged with that of the remaining XIS detectors (Fig. 6), even when the photon index of the power-law continuum was allowed to vary between detectors. As the XIS 0, 2 and 3 (FI) were all self-consistent, this divergence was possibly caused by calibration effects around the oxygen K detector edge.

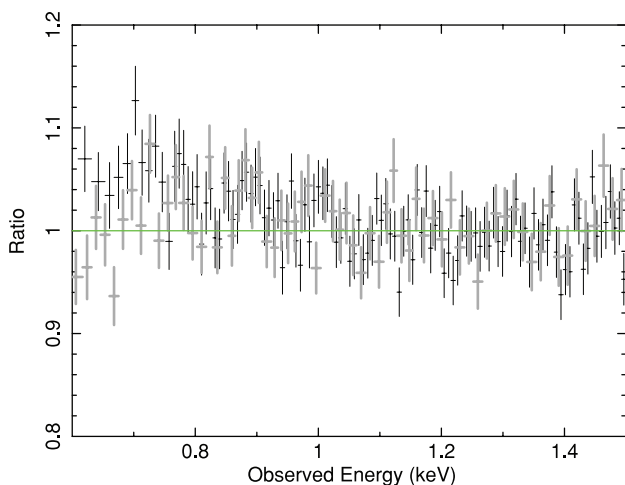


**Figure 6.** A ratio plot showing the divergence of the XIS 1 detector data (light grey) with that of the XIS 0, 2 and 3 detectors (black) in the soft X-ray regime (see Section 3.2).

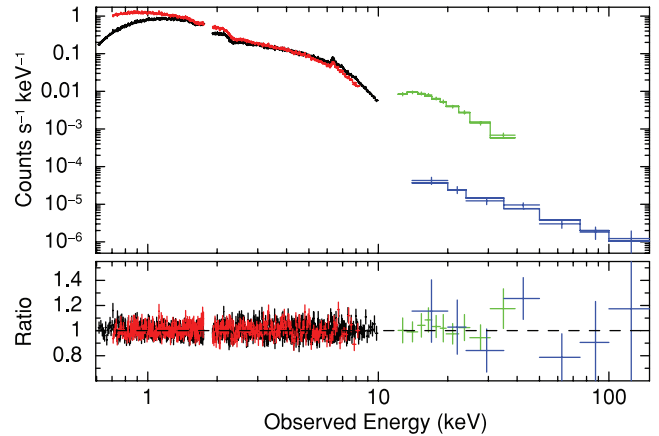


**Figure 7.** The broad-band spectra of NGC 7213 (in the observed frame) with the inclusion of the *Swift* BAT spectra (blue). A plot of the ratio of the residuals to the model described in Section 3.2 and Table 2 is shown in the lower panel. No significant residuals are present.

To account for this, the data from the XIS 1 detector were ignored below 0.7 keV.

In an attempt to then model the observed soft excess, we added a *MEKAL* thermal plasma component incorporating the emission spectra from a hot diffuse gas (Starling et al. 2005). It is worth noting that a featureless blackbody component models the soft excess with an equally good fit as there are no strong lines. However, this model was not considered any further as the lack of evidence for a strong BBB (Wu et al. 1983) suggested little thermal emission directly from the disc (Starling et al. 2005). The addition of the *MEKAL* component gave a best-fitting thermal plasma temperature of  $k_B T = 0.27^{+0.05}_{-0.04}$  keV and resulted in an overall better fit with  $\chi^2/\text{d.o.f.} = 1104/1022$  compared to 1151/1024 before the *MEKAL* component was added.<sup>3</sup> The luminosity of the *MEKAL* component was calculated at  $L = 2.14 \times 10^{40}$  erg s<sup>-1</sup> corresponding to only 1 per cent of the total luminosity in the 0.5–10 keV band. As no further significant residuals were observed in the spectra (Fig. 7), this became our accepted broad-band model, the final parameters of which are summarized in Table 2 (note that the full broad-band model from 0.6 to 150 keV also resulted in a tighter constraint on the reflection scaling factor,  $R$ , the best-fitting value of which is shown in Table 2). A plot of the relative unfolded model contributions is shown in Fig. 8.

### 3.3 Comparison with past observations

#### 3.3.1 *XMM-Newton* and *BeppoSAX*

We tested for any long-term variations in the source by applying our best-fitting broad-band *Suzaku* model to the 2001 simultaneous *XMM-Newton* (30 ks exposure) and *BeppoSAX* PDS (38 ks exposure) observations (May 2001; see Table 3), as published previously by Bianchi et al. (2003, 2004) and Starling et al. (2005). The ratio of the *XMM-Newton* EPIC-pn spectrum from 0.3 to 10 keV to the best-fitting *Suzaku* model, with continuum parameters described in Table 2, is shown in Fig. 9. It can be seen that compared to the

<sup>3</sup> Modelling the soft excess with an *APEC* component was also considered (<http://hea-www.harvard.edu/APEC/>; Smith et al. 2001) although at the *Suzaku* resolution here, the fit was identical to that obtained with the *MEKAL* thermal plasma.

**Table 2.** Spectral parameters of the continuum fit in the 0.6–150 keV range (see Section 3.2 for details).

Model component	Fit parameter	Value
1. Cut-off power law <sup>a</sup>	$\Gamma$	$1.74 \pm 0.01$
	High-energy cut-off	$>350$
	Normalization	$6.28^{+0.05}_{-0.03}$
2. Galactic absorption <sup>b</sup>	$N_{\text{H}}$	$1.10 \times 10^{20}$
3. PEXRAV <sup>c</sup>	$ R $	$0.09^{+0.19}_{-0.08}$
4. MEKAL <sup>d</sup>	$k_{\text{B}}T$	$0.27^{+0.05}_{-0.04}$
	Normalization	$1.27^{+0.59}_{-0.38}$
	Luminosity	$2.14 \times 10^{40}$
5. Fit statistics <sup>e</sup>	$\chi^2/\text{d.o.f.}$	1100/1041
	Null probability	$4.40 \times 10^{-2}$

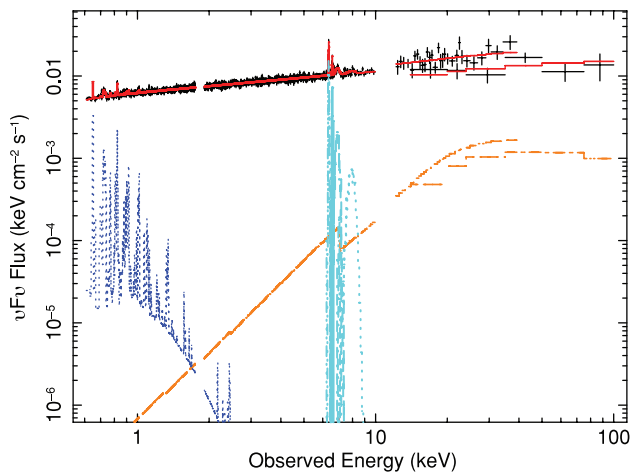
<sup>a</sup>  $\Gamma$ , photon index; high-energy cut-off in units of keV; normalization in units of  $\times 10^{-3}$  photon  $\text{cm}^{-2} \text{s}^{-1}$ .

<sup>b</sup> Local Galactic absorption (at  $z = 0$ ), units  $\text{cm}^{-2}$ .

<sup>c</sup>  $|R|$ , reflection scaling factor, where a value  $R = 1$  corresponds to reflection from neutral material subtending  $2\pi$ sr.

<sup>d</sup>  $k_{\text{B}}T$ , plasma temperature in units of keV; normalization (emission measure =  $\int n_e n_{\text{H}} dV$ ) in units of  $\times 10^{63} \text{cm}^{-3}$ .

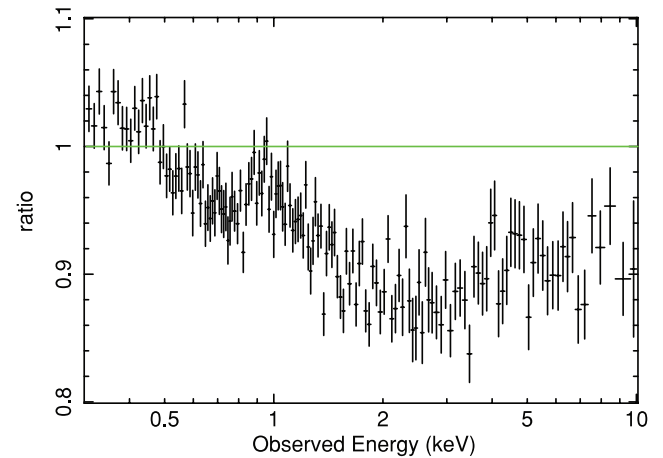
<sup>e</sup> Reduced chi-squared ( $\chi^2/\text{d.o.f.}$ ) and null hypothesis probability for spectral fit.


**Figure 8.** A plot showing the relative contributions of the individual model components across the broad-band 0.6–100 keV *Suzaku*+BAT energy range (see Section 3.2 for details). The PEXRAV neutral reflection component is shown in orange over the 1–100 keV energy range whilst the soft collisionally ionized MEKAL component (at energies  $<3$  keV) is shown in navy blue. The emission in the Fe K complex is modelled with individual Gaussians. The red curve spanning the whole energy range shows the sum of all the model components (including the absorbed power-law continuum) superimposed on the data.

*Suzaku* XIS spectrum, the pn spectrum is steeper, while overall the flux was slightly lower in the *XMM-Newton* data with a value of  $2.19 \times 10^{-11} \text{erg cm}^{-2} \text{s}^{-1}$  over the 2–10 keV energy range. We also note that the flux obtained from the *BeppoSAX* data was lower than that obtained with the *Suzaku* HXD over the 12–100 keV range ( $2.46 \times 10^{-11}$  compared to  $3.81 \times 10^{-11} \text{erg cm}^{-2} \text{s}^{-1}$ , respectively). Since the photon index of the power-law continuum is quite hard in this source, this difference could simply arise from small changes in the intrinsic power law. The model is generally in good agreement with the data although subtle changes in the continuum can be observed, with the spectral curvature being more apparent in the

**Table 3.** Log of observations of NGC 7213 (see Section 3.3 for details).

Date	Mission	Instrument	Exposure (ks)
27/05/2001	<i>BeppoSAX</i>	MECS	61
		PDS	38
29/05/2001	<i>XMM-Newton</i>	EPIC-PN	30
15/12/2004 to 27/10/2006	<i>Swift</i>	BAT	2300
22/10/2006	<i>Suzaku</i>	XIS/HXD	90
06/08/2007	<i>Chandra</i>	HETG	148


**Figure 9.** Data/model residuals of the 2001 *XMM-Newton* EPIC-pn data to the *Suzaku* model listed in Table 2. The *XMM-Newton* data show the source to have a slightly steeper spectrum compared to *Suzaku* at energies below 2 keV, while overall the continuum flux in the 2–10 keV band is lower in the *XMM-Newton* data in 2001 compared to *Suzaku* in 2006 (see Section 3.3 for details).

*XMM-Newton* data, e.g. with the spectrum being noticeably steeper below 2 keV, but somewhat flatter above 3 keV. No strong residuals are present in the iron K band, which suggests that the iron line emission has remained constant between the 2001 *XMM-Newton* and 2006 *Suzaku* observations.

To quantify the changes in the spectrum, the single power-law continuum used to fit the *Suzaku* data in Sections 3.1 and 3.2 was replaced with a broken power law, breaking at  $2.19^{+0.34}_{-0.30}$  keV with  $\Gamma$  values of  $1.84 \pm 0.01$  and  $1.71 \pm 0.02$  below and above this energy break, respectively. Furthermore, a slight softening of the spectrum below 1 keV in the *XMM-Newton* data, as suggested by the bump in the residuals around 0.9 keV (which may be due to the Ne IX triplet or a blend of emission from iron L-shell lines), indicates that the single-temperature MEKAL component obtained from the *Suzaku* data was not sufficient to model the soft excess. Thus, a second MEKAL component was added to the model with a higher temperature of  $k_{\text{B}}T = 0.86^{+0.20}_{-0.14}$  keV, which significantly improved the fit ( $\Delta\chi^2 = 19.2$ ) compared to the model with only a single-temperature plasma. The fit parameters of this best-fitting model to the *XMM-Newton* data are summarized in Table 4.

For consistency, this two-temperature MEKAL model was then applied to the 2006 *Suzaku* data set. The temperatures and normalizations of the MEKAL were kept fixed at the best-fitting values from the *XMM-Newton* data, as an extended diffuse collisional plasma may not be expected to vary significantly over time (note that if the parameters are allowed to vary, the values obtained from *Suzaku* are consistent with the *XMM-Newton* data, within the errors). The broken-power-law continuum parametrization was also

**Table 4.** Spectral parameters of the broad-band fit in the 0.6–150 keV energy range for the 2006 *Suzaku* and 2001 simultaneous *XMM–Newton* and *BeppoSAX* observations (see Section 3.3 for details). The Fe-line complex parameters from the 2007 *Chandra* HETG observation (reported by Bianchi et al. 2008) are also shown for ease of comparison.

Model component	Fit parameter	<i>Suzaku</i>	<i>XMM–Newton</i> and <i>BeppoSAX</i>	<i>Chandra</i> HETG
Flux <sup>a</sup>	$F_{0.5-2}$	1.37	1.29	-
	$F_{2-10}$	2.44	2.19	-
	$F_{12-100}$	3.81	2.46	-
Broken power law <sup>b</sup>	$\Gamma_1$	$1.94^{+0.09}_{-0.06}$	$1.84 \pm 0.01$	-
	$E_{\text{break}}$	$0.93^{+0.06}_{-0.07}$	$2.19^{+0.34}_{-0.30}$	-
	$\Gamma_2$	$1.74 \pm 0.01$	$1.71 \pm 0.02$	-
	Normalization	$6.11^{+0.09}_{-0.16}$	$5.92^{+0.03}_{-0.04}$	-
MEKAL <sup>c</sup>	$k_{\text{B}}T_1$	FIXED	$0.24^{+0.07}_{-0.06}$	-
	Norm <sub>1</sub>	FIXED	$6.60^{+4.06}_{-3.81}$	-
	$k_{\text{B}}T_2$	FIXED	$0.86^{+0.20}_{-0.14}$	-
	Norm <sub>2</sub>	FIXED	$7.63^{+2.74}_{-2.65}$	-
	$L_{\text{total}}$	1.99	1.99	-
Fe K $\alpha$ line <sup>d</sup>	$E_{\text{K}\alpha}$	$6.39 \pm 0.01$	$6.40 \pm 0.02$	$6.40 \pm 0.01$
	EW <sub>K<math>\alpha</math></sub>	$83.1^{+11.0}_{-10.7}$	$85.9^{+14.0}_{-14.4}$	$120^{+40}_{-30}$
	Line flux <sub>K<math>\alpha</math></sub>	$2.18^{+0.28}_{-0.29}$	$2.33^{+0.38}_{-0.39}$	$2.9^{+0.9}_{-0.7}$
6.60 keV line <sup>d</sup>	$E_{6.60}$	$6.60 \pm 0.03$	$6.66^{+0.04}_{-0.05}$	$6.72^{+0.01}_{-0.02}$
	EW <sub>6.60</sub>	$24.1 \pm 7.9$	$27.4 \pm 11.6$	$24 \pm 17$
	Line flux <sub>6.60</sub>	$0.67 \pm 0.22$	$0.78 \pm 0.33$	$0.7 \pm 0.5$
6.95 keV line <sup>d</sup>	$E_{6.95}$	$6.95 \pm 0.03$	$6.91 \pm 0.08$	$6.99^{+0.02}_{-0.01}$
	EW <sub>6.95</sub>	$62.3^{+16.0}_{-14.2}$	$37.1 \pm 18.8$	$60 \pm 30$
	Line flux <sub>6.95</sub>	$1.40^{+0.36}_{-0.32}$	$0.89 \pm 0.45$	$1.3 \pm 0.6$
Statistics	$\chi^2/\text{d.o.f.}$	747/723	846/872	-
	Null probability	0.26	0.73	-

<sup>a</sup> Continuum flux in the specified range in units of  $\times 10^{-11}$  erg cm<sup>-2</sup> s<sup>-1</sup>.

<sup>b</sup>  $\Gamma$ , photon index;  $E_{\text{break}}$  in units keV; normalization in units of  $\times 10^{-3}$  photon cm<sup>-2</sup> s<sup>-1</sup>.

<sup>c</sup>  $k_{\text{B}}T$ , plasma temperature in units of keV; normalization ( $= \int n_e n_{\text{H}} dV$ ) in units  $\times 10^{62}$  cm<sup>-3</sup>; total MEKAL luminosity from 0.5 to 10 keV in units of  $10^{40}$  erg s<sup>-1</sup>. All MEKAL fit parameters in the *Suzaku* data set are fixed at the best-fitting values from the XMM data.

<sup>d</sup>  $E_{\text{line}}$ , line energy in units of keV; EW, equivalent width in units of eV; line flux in units of  $\times 10^{-5}$  photon cm<sup>-2</sup> s<sup>-1</sup>.

retained from the *XMM–Newton* fit, although the photon indices and normalizations were allowed to vary. A comparison of fit parameters for the *Suzaku* and *XMM–Newton* observations is shown in Table 4. No other significant variations were observed between the two observations; the Fe K line parameters appear to be consistent with constant values (within the errors) for the centroid energies and line fluxes, while the 2001 *BeppoSAX* PDS data show no evidence for a reflection hump above 10 keV (with  $R < 0.2$ ; see also Bianchi et al. 2004), consistent with what is found by the *Suzaku* HXD. Furthermore, the lower limit on the high-energy cut-off value is also constrained to  $>300$  keV (see also Dadina 2008), in good agreement with the HXD and *Swift* BAT.

### 3.3.2 *Chandra* HETG

The emission line at 6.60 keV in the *Suzaku* XIS spectrum is found to be rejected at the  $>99.9$  per cent confidence level as arising from the resonance transition of helium-like iron (see Section 3.1 and Fig. 5). As a consistency check, we modelled the archival *Chandra* HETG spectrum (using the latest version of the calibration data base; v.4.2.2) at Fe K with an absorbed power law and parametrized the emission lines with simple Gaussians consistent with the values found by Bianchi et al. (2008) (also see Table 4) with emission lines at 6.40, 6.72 and 6.99 keV. Fixing an additional narrow line

( $\sigma = 10$  eV) at 6.60 keV (as required by *Suzaku*) in the HETG spectrum was not required by the data but resulted in a value for the equivalent width of  $\text{EW} < 21.2$  eV, which is consistent with the equivalent width of  $\text{EW} = 24.4 \pm 8.0$  eV found in the *Suzaku* XIS. Likewise, including a narrow Gaussian in the *Suzaku* spectrum with the centroid energy fixed at 6.72 keV (as found by *Chandra*) is also not required by the XIS data but yields an upper limit on the equivalent width of  $\text{EW} < 14.3$  eV, again consistent with the equivalent width of  $\text{EW} = 24.0 \pm 17.0$  eV found by Bianchi et al. (2008) with the *Chandra* HETG. Therefore, it appears that the Fe K parameters in both data sets are consistent with each other with no evidence of variability detected within the errors.

## 4 DISCUSSION

In this section, the possible origin of both the neutral and ionized iron K line emission from NGC 7213 is discussed along with its implications for the nature of the central engine in this source.

### 4.1 The origin of the neutral Fe K $\alpha$ line

We first investigated the possibility of whether a distant Compton-thick reflector, e.g. such as the pc-scale torus, could account for the neutral Fe K $\alpha$  emission. The tight constraint on the reflection

fraction of  $R = 0.09^{+0.19}_{-0.08}$ , obtained in Section 3.2 (also see Table 2), appears to rule out the possibility of the 6.39 keV line originating via scattering off Compton-thick matter since, for an Fe  $K\alpha$  line with an equivalent width of  $\sim 80$  eV (as observed here), a strong reflection scaling factor value of  $R \approx 0.6$  would be required (George & Fabian 1991). To test this further, the ionized reflection model REFLIONX (Ross & Fabian 2005) was used in place of the simple 6.39 keV Gaussian emission and PEXRAV model for the Compton-scattered continuum off neutral material. The other model components, as described in Section 3.2 (also see Tables 1 and 2), were adopted and are identical in the spectral fits. The REFLIONX model consists of the emergent spectrum for a photoionized optically thick slab of gas when irradiated by a power-law spectrum, with a high energy exponential cut-off of 300 keV, using the abundances of Anders & Ebihara (1982). The advantage of the REFLIONX model is that it self-consistently computes both the reflected continuum and line emission for the astrophysically abundant elements.

We initially fixed the iron abundance to Solar, while the redshift of the reflector was found to be consistent with the cosmological redshift of the source, with no net (e.g. gravitational) redshift. Given the narrow unresolved iron  $K\alpha$  emission observed in the *Suzaku* spectrum, no additional velocity broadening was applied to the reflected spectrum. We also fixed the reflector ionization parameter<sup>4</sup> at a value of  $\xi = 10 \text{ erg cm s}^{-1}$  (the lowest value allowed by the model), corresponding to near-neutral iron (i.e. iron atoms typically in a low ionization state corresponding to Fe I–XVII). This model provides an upper limit on the reflection scaling factor of  $R < 0.16$ , consistent with what was found by the PEXRAV model in Section 3, but results in a relatively poor fit to the *Suzaku*+BAT data of  $\chi^2/\text{d.o.f.} = 810/715$  (null probability =  $7.22 \times 10^{-3}$ ). This is due to the fact that the model underpredicts the amount of iron  $K\alpha$  emission, leaving a significant positive residual at  $\sim 6.4$  keV in the *Suzaku* XIS data. Allowing the Fe abundance to vary to enhance the iron K emission results in an acceptable fit of  $\chi^2/\text{d.o.f.} = 745/714$  corresponding to a null hypothesis probability of 0.21 (with  $R < 0.06$ ). However, in order to adequately model the iron  $K\alpha$  line, this requires an overabundance of Fe by a factor of  $\sim 10$  with respect to Solar (the 90 per cent confidence lower limit on this value is still four times Solar).

It therefore appears that the lack of an observed Compton reflection hump in the data above 10 keV means that the reflection and Fe  $K\alpha$  emission cannot be simultaneously modelled in this way, seemingly ruling out a reflection origin for the Fe  $K\alpha$  emission, as also suggested by Bianchi et al. (2003) on the basis of the *BeppoSAX* data. Indeed, an acceptable fit can only be obtained if the abundances are assumed to be greatly super-Solar, at odds with the modest spread of values found by Perola et al. (2002) from a sample of nine bright type I Seyferts and narrow emission-line galaxies (NELGs) observed with *BeppoSAX*. Thus, it appears unlikely that the 6.39 keV emission originates via reflection off Compton-thick matter unless the material covers a very small solid angle ( $< 1$  sr) and is extremely iron overabundant.

Instead, it is perhaps more likely that the near-neutral iron  $K\alpha$  line originates in Compton-thin matter, covering a higher fraction of  $4\pi$  steradians solid angle. Indeed, an estimate of the column density of the  $K\alpha$ -emitting material can be made using the calculations

of Yaqoob et al. (2010) where an analytic expression relating the efficiency of the Fe  $K\alpha$  line production and the column density of the emitting material is derived in the optically thin limit. The production efficiency of the Fe  $K\alpha$  line is calculated by

$$\chi_{\text{Fe } K\alpha} = \frac{I_{\text{Fe } K\alpha, n}}{\int_{E_K}^{\infty} E^{-\Gamma} dE}, \quad (1)$$

where  $E_K$  is the threshold energy for Fe K-shell absorption and  $I_{\text{Fe } K\alpha, n}$  refers to the line flux renormalized to an incident continuum with a flux of  $1 \text{ photon cm}^{-2} \text{ s}^{-1} \text{ keV}^{-1}$  at 1 keV.  $\Gamma$  is the photon index assuming an incident power-law continuum. Adopting the Verner et al. (1996) value for  $E_K$  of 7.124 keV, we calculate an Fe  $K\alpha$  line production efficiency of  $\sim 1$  per cent for NGC 7213. In the Compton-thin case, we find that this results in an estimate on the column density of the  $K\alpha$ -emitting material of  $N_H \sim 2 \times 10^{23} \text{ cm}^{-2}$  using the analytic expression derived by Yaqoob et al. (2010) (equation 4 in the aforementioned publication). Although this value is consistent with that found by Bianchi et al. (2008), the expression is valid only in the Compton-thin limit which begins to break down for  $N_H > 2 \times 10^{22} \text{ cm}^{-2}$  as the optical depth of the Fe K line photons to absorption and scattering becomes non-negligible (see Yaqoob et al. 2010, Fig. 2). However, accounting for these effects, according to the calculations of Yaqoob et al. (2010) and Murphy & Yaqoob (2009), a column density of  $N_H \sim 3\text{--}4 \times 10^{23} \text{ cm}^{-2}$  can result in an Fe  $K\alpha$  line efficiency of 1 per cent for a face-on geometry covering  $2\pi$  sr in their toroidal X-ray reprocessor model. Thus, the Fe  $K\alpha$  line may originate in a Compton-thin torus or perhaps the outer BLR clouds, as suggested by Bianchi et al. (2005), although the covering fraction would perhaps be slightly high in the latter case (Netzer & Laor 1993).

#### 4.2 The origin of the highly ionized Fe

We investigated the possibility of an ionized accretion disc as a potential origin for the 6.60 and 6.95 keV emission lines. To test this scenario, we attempted to model the two ionized emission lines by a REFLIONX component with a high ionization parameter of  $\log \xi = 3.0^{+0.2}_{-0.1} \text{ erg cm s}^{-1}$ . The remainder of the *Suzaku* spectrum was modelled as before, i.e. a cut-off power law for the continuum emission, a single-temperature thermal MEKAL component for the weak soft X-ray excess and a narrow Gaussian centred at 6.39 keV for the neutral iron  $K\alpha$  emission. No relativistic blurring was applied. This resulted in a poor fit of  $\chi^2/\text{d.o.f.} = 791/717$  (null probability =  $2.79 \times 10^{-2}$ ) with the model unable to account for the ionized emission from either Fe xxv or Fe xxvi (see Fig. 10). Indeed, due to the large intrinsic electron scattering depth at such high values of  $\xi$ , the lines in the reflection model become too broadened and so are unable to model the relatively narrow 6.60 and 6.95 keV lines that are observed in the *Suzaku* spectrum. Furthermore, the 90 per cent confidence upper limit on the reflection fraction for the highly ionized reflector is restricted to  $R < 0.06$ , which seemingly allows us to reject the presence of a highly ionized Compton-thick medium in NGC 7213, such as a highly ionized, but Compton-thick inner accretion disc.

In addition, the inability to model the neutral Fe  $K\alpha$  emission with a low ionization reflector (see Section 4.1) coupled with the apparent lack of a Compton hump  $> 10$  keV means that this source exhibits no evidence at all for any Compton-thick material, either neutral or ionized. Furthermore, the data do not appear to show any relativistic signatures since the neutral and ionized iron lines appear to be narrow (or only moderately broad in the case of Fe xxvi), thus ruling out any emission from the innermost regions around

<sup>4</sup> Note that in the REFLIONX ionized reflection model the ionization parameter is defined as  $\xi = 4\pi F/n$  and has units  $\text{erg cm s}^{-1}$ , where  $F$  is the illuminating flux incident upon the reflector (integrated over the energy range 100 eV to 1 MeV) and  $n$  is the gas density in  $\text{cm}^{-3}$ .

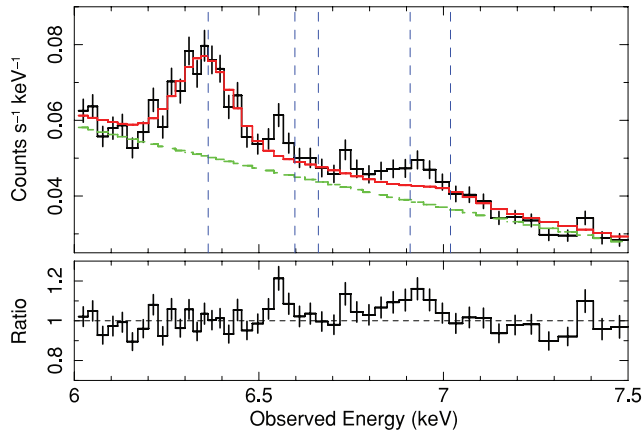


**Figure 10.** A plot showing the inability to model the highly ionized Fe emission at 6.60 and 6.95 keV with an ionized reflector, therefore suggesting a non-reflection origin for these lines (as described in Section 4.2). The continuum level is shown in green and the lower panel shows the ratio of the residuals to the model. The neutral  $K\alpha$  line at 6.39 keV is modelled with a Gaussian. The vertical dotted lines show the expected line energies of, from left to right, Fe  $K\alpha$ , Fe xxv forbidden, Fe xxv 1s–2p resonance, Fe xxvi 1s–2p and Fe  $K\beta$  in the observed frame.

the black hole. Combining the lack of evidence for any Compton-thick matter in this source with the lack of any relativistic signature seems to suggest the complete absence of an inner optically thick accretion disc in NGC 7213. Instead, it may support the notion of an accretion disc which is truncated at some radius with the inner regions replaced by some form of radiatively inefficient accretion flow (RIAF; Narayan & Yi 1995), where the low efficiency of the inner, hot corona leads to much of the energy being advected into the black hole rather than radiated away.

#### 4.2.1 Collisionally ionized model

We instead investigated the possibility of a collisionally ionized origin for the highly ionized Fe K emission which we modelled with a high-temperature broadened APEC component (Smith et al. 2001). This required a temperature of  $k_B T = 13.03^{+2.61}_{-2.86}$  keV and velocity broadening,  $\sigma \sim 2500$  km s<sup>-1</sup>, resulting in a fit statistic of  $\chi^2/\text{d.o.f.} = 788/716$ . Inspection of the data around the iron K band reveals that the collisionally ionized model overpredicts the contribution of the resonance line compared to the forbidden line of Fe xxv, which leaves some excess line flux near 6.60 keV unmodelled, although the Fe xxvi line is modelled well. Thus, although the collisional model cannot be ruled out with high confidence in the present data, given that the energy of the 6.60 keV line appears more consistent with the forbidden rather than resonance transition of Fe xxv, an additional photoionized component would perhaps be required to model this line (see Section 4.2.2).

An estimate on the density of the collisionally ionized material can be calculated from the normalization of the APEC code, which returns  $\int n^2 dV \sim 10^{64}$  cm<sup>-3</sup>. If the observed broadening of the line is assumed to be due to a Keplerian orbit ( $\sigma \sim 0.1$  keV corresponding to a few  $\times 10^4$  km s<sup>-1</sup>; see Table 1), we can calculate an estimate on the radius of the emitting material from the central black hole of a few  $\times 10^4 R_g$ , where  $1 R_g = 1.5 \times 10^{13}$  cm for a black hole mass of  $10^8 M_\odot$  (Nelson & Whittle 1995). Adopting this radius of  $R \sim 1.5 \times 10^{17}$  cm results in an estimate of  $n \sim 10^6$  cm<sup>-3</sup> for the density of the emitting material.

If the collisional gas is indeed responsible for some of the highly ionized Fe emission, then we note that the conditions of the gas must be different from those in the lower temperature gas used to model the weak soft excess at energies  $< 1$  keV (see Section 3.2). The two components require very different temperatures ( $0.27^{+0.05}_{-0.04}$  and  $13.03^{+2.61}_{-2.86}$  keV for the low- and high-temperature gases, respectively) and we note that any contribution from one distinct zone of emission to the other is negligible (i.e. no significant emission from the lower temperature zone is found to be contributing the emission at Fe K and vice versa). However, the two zones of gas could be linked by their origin albeit on completely different scales with the emission from the lower temperature gas originating at a much greater distance from the black hole.

#### 4.2.2 A photoionization model for the ionized iron K emission

An alternative origin for the lines could be emission from a photoionized, but Compton-thin plasma. We modelled this scenario using the xSTAR 2.1ln11 code (Kallman & McCray 1982), which incorporates the abundances of Grevesse, Noels & Sauval (1996). We initially modelled the lines using a single zone of emission with Solar abundances and a turbulent velocity width of 200 km s<sup>-1</sup>. The best-fitting value of the ionization parameter was  $\log \xi = 3.7 \pm 0.3$  (where the ionization parameter in xSTAR is defined as in equation 3), which resulted in an acceptable fit with  $\chi^2/\text{d.o.f.} = 779/715$  (null probability =  $4.73 \times 10^{-2}$ ). Even so, some slight excess residuals were apparent, particularly around the 6.95 keV line, which might suggest there is some intrinsic velocity broadening of the ionized lines. For instance, as measured from Section 3.1, the H-like line appears to have an FWHM of  $\sim 10000$  km s<sup>-1</sup>.

Thus, an alternative xSTAR grid was used with a higher turbulence velocity of  $\sigma = 3000$  km s<sup>-1</sup>. This resulted in a slightly better fit of  $\chi^2/\text{d.o.f.} = 765/715$  (null probability =  $8.50 \times 10^{-2}$ ), with an ionization parameter of  $\log \xi = 4.4 \pm 0.1$  (see Section 4.3.3 for a calculation of the lower limit on the column density). This fit is significantly better than the one obtained with the collisionally ionized model (Section 4.2.1) with  $\Delta\chi^2 = 23$  between the two models. A plot of this model superimposed on the data is shown in Fig. 11. We also calculated the 90 per cent uncertainty on the redshift of the zone allowing us to constrain the net velocity shift of the ionized emitter to be  $v = +650^{+1650}_{-1500}$  km s<sup>-1</sup>, where a positive velocity denotes redshifted/infalling material. Thus, the data do not formally require a velocity shift in this model. Further zones of ionized matter are also not required by the data.

Both high and low turbulence models appear to give good fits over the iron K band, with the 6.95 keV emission line originating from the Fe xxvi Ly $\alpha$  doublet and the 6.60 keV He-like line arising due to a blend of the forbidden and intercombination lines at 6.637 and 6.668 keV, respectively. In the low-density limit assumed in the xSTAR model here (where  $n < 10^{16}$  cm<sup>-3</sup>), the He-like emission is from an approximately equal mixture of the forbidden and intercombination lines, with a negligible contribution from the resonance line at 6.700 keV. Note that some weak emission via satellite lines of lower ionization iron (i.e. Fe xxiii–xxiv) could also be contributing to this blend of emission although at the high ionization parameter inferred here (of  $\log \xi \sim 4$ ), this contribution is likely to be negligible (Kallman & McCray 1982). However, future calorimeter-based spectroscopy, e.g. with Astro-H, will be required to spectrally resolve all the line emission components associated with the He-like triplet of iron and to constrain the intrinsic velocity broadening.

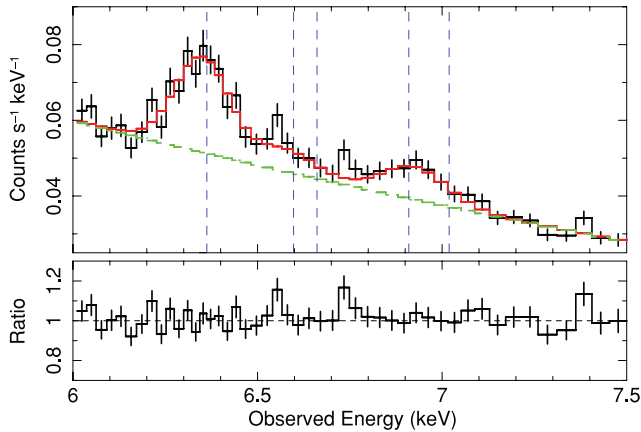


**Figure 11.** A plot showing the fit obtained when the highly ionized Fe is modelled with a photoionized *xstar* grid with  $\sigma = 3000 \text{ km s}^{-1}$  and  $\log \xi = 4.4 \text{ erg cm s}^{-1}$  (as described in Section 4.2.2). The continuum level is shown in green and the lower panel shows the ratio of the residuals to the model. The neutral Fe  $K\alpha$  line at 6.39 keV is modelled with a Gaussian. The vertical dotted lines show the expected line energies of, from left to right, Fe  $K\alpha$ , Fe xxv forbidden, Fe xxv 1s–2p resonance, Fe xxvi 1s–2p and Fe  $K\beta$  in the observed frame.

We also note that if the highly ionized iron lines are originating in photoionized gas, then the possibility remains that a similar photoionized gas but with a much lower ionization parameter could be responsible for the weak soft X-ray lines observed at energies  $< 1 \text{ keV}$ . However, Starling et al. (2005) analysed the results of an *XMM-Newton* RGS observation of NGC 7213 and found that a collisionally ionized thermal plasma was preferred by the data from consideration of the ‘*G*’ ratio (Porquet & Dubau 2000) of the O VII triplet.

#### 4.2.3 The location of the highly ionized gas

From the consideration of various photoionized and collisionally ionized models, it appears that the 6.60 and 6.95 keV lines are consistent with originating in a photoionized medium, although the H-like  $\text{Ly}\alpha$  line appears to be quite strong with an equivalent width of  $\sim 60 \text{ eV}$ . Bianchi & Matt (2002) calculate the equivalent widths of Fe xxv and Fe xxvi lines with respect to both the reflected and total continua and show that an equivalent width of  $\sim 15 \text{ eV}$  for H-like Fe would be expected if it originated in material of column density,  $N_{\text{H}} \sim 10^{23} \text{ cm}^{-2}$ , with an ionization parameter of  $\log \xi \sim 3.5$ , photon index of  $\Gamma = 1.7$  and a covering fraction,  $f = 1$ . To test whether our equivalent width of  $\sim 60 \text{ eV}$  was feasible we calculated a lower limit on the column density of the photoionized material in the case of one single zone of emission.

For a uniform, spherical, Compton-thin shell, the normalization of the photoionized emission component is defined within the *xstar* code by<sup>5</sup>

$$k = f_{\text{cov}} \frac{L_{\text{ion}}}{D^2}, \quad (2)$$

where  $f_{\text{cov}}$  is the covering fraction of the material (i.e.  $f_{\text{cov}} = 1$  for matter covering  $4\pi \text{ sr}^{-1}$ ),  $L_{\text{ion}}$  is the ionizing luminosity in units  $10^{38} \text{ erg s}^{-1}$  from 1 to 1000 Rydbergs and  $D$  is the distance to the source in kpc. Physically, the *xstar* normalization is simply

proportional to the observed X-ray flux of the source multiplied by the covering fraction of the photoionized gas. Thus, the appropriate value of this normalization,  $k$ , for NGC 7213 can be calculated assuming a covering fraction of 1. For the luminosity and distance of NGC 7213, this results in a value of  $k = 9.0 \times 10^{-5}$  in units  $10^{38} \text{ erg s}^{-1} \text{ kpc}^{-2}$ , where we have adopted a distance of 25 000 kpc to NGC 7213 (Mould et al. 2000). The value used for the ionizing luminosity was derived from an extrapolation of the broken power-law continuum in Table 4, integrated from 1 to 1000 Rydbergs and is found to be  $5.61 \times 10^{42} \text{ erg s}^{-1}$ , comparable to the estimate of the bolometric luminosity of  $\sim 9 \times 10^{42} \text{ erg s}^{-1}$  by Starling et al. (2005).

In the model used in Section 4.2.2, we have fixed the normalization of the additive *xstar* emission component to the above value and thus assumed a fully covering shell of gas around NGC 7213, with the appropriate source luminosity and distance from above. The column density was then allowed to vary within the *xstar* model, in order to fit the ionized iron K emission lines. This provided a best-fitting value for the column density of  $N_{\text{H}} = 4.0_{-0.8}^{+0.5} \times 10^{23} \text{ cm}^{-2}$ . The 90 per cent confidence lower limit on the column density is  $N_{\text{H}} > 3.2 \times 10^{23} \text{ cm}^{-2}$  for a fully covering spherical shell of gas, with an ionization parameter of  $\log \xi \sim 4$  as above. For a shell that does not fully cover the source, then the column density will need to be higher to compensate for the lower covering. This is in good agreement with the calculations of Bianchi & Matt (2002), who predict an equivalent width for Fe xxvi  $\text{Ly}\alpha$  of 15 eV for a column density of  $10^{23} \text{ cm}^{-2}$ , compared to the observed 60 eV equivalent width in the case of NGC 7213, but for a column density approximately three to four times higher.

In order to better constrain the origin of the Fe xxvi  $\text{Ly}\alpha$  line, it is important to estimate a value for the distance of the emitting material. Assuming a uniformly ionized, spherical shell of gas, the ionization parameter in *xstar* is defined as

$$\xi = \frac{L_{\text{ion}}}{nR^2} \quad (3)$$

and has units  $\text{erg cm s}^{-1}$  where  $L_{\text{ion}}$  is the ionizing luminosity from 1 to 1000 Rydbergs,  $n$  is the gas density in  $\text{cm}^{-3}$  and  $R$  is the radius of the absorbing/emitting material from the central source of X-rays. Combining this with the column density which is given by

$$N_{\text{H}} = \int_{R_{\text{in}}}^{\infty} n \, dR \quad (4)$$

yields an estimate on the inner radius of the emitting material:

$$R_{\text{in}} \sim \frac{L_{\text{ion}}}{N_{\text{H}} \xi}. \quad (5)$$

Assuming values of  $L_{\text{ion}} \sim 5 \times 10^{42} \text{ erg s}^{-1}$  (derived above),  $\xi \sim 5000$  and  $N_{\text{H}} \sim 3 \times 10^{23} \text{ cm}^{-2}$  then gives a lower limit on  $R$  of  $\sim 3 \times 10^{15} \text{ cm}$  corresponding to a value of  $\sim 200 R_{\text{g}}$  (assuming a black hole mass of  $10^8 M_{\odot}$ ; Nelson & Whittle 1995) and infers an electron density of  $n_{\text{e}} \sim 10^8 \text{ cm}^{-3}$  (equation 3). This radius is also consistent with the FWHM of  $\sim 10000 \text{ km s}^{-1}$  of the H-like Fe line which, if the broadening is assumed to be the intrinsic broadening due to a Keplerian orbit, provides an estimate on the line emitting radius of a few  $\times 10^3 R_{\text{g}}$ .

### 4.3 NGC 7213 as a low-luminosity AGN

#### 4.3.1 The inner advective flow in NGC 7213

From 2 to 10 keV, the X-ray spectrum of NGC 7213 resembles that of a typical type 1 Seyfert galaxy where the spectrum is dominated

<sup>5</sup> See <http://heasarc.gsfc.nasa.gov/docs/software/xstar/docs/html/node94.html>.

by a power-law continuum of  $\Gamma = 1.75$  and near-neutral Fe K $\alpha$  emission at 6.39 keV. This neutral K $\alpha$  emission may originate from Compton-thin material of  $N_{\text{H}} \sim 3\text{--}4 \times 10^{23} \text{ cm}^{-2}$  possibly in the outer BLR or a Compton-thin torus (Bianchi et al. 2008). We also detect significant emission from highly ionized material located close to the central source with Fe xxv and Fe xxvi perhaps originating in a photoionized medium with a column density  $N_{\text{H}} \gtrsim 3 \times 10^{23} \text{ cm}^{-2}$  invoked to match the high observed EW of  $\sim 60 \text{ eV}$ . This emission is likely to originate at a distance of  $R \sim 10^3\text{--}10^4 R_{\text{g}}$  from the black hole/X-ray source.

Given the tight constraints on reflection from both neutral and ionized material ( $R < 0.16$  and  $R < 0.06$ , respectively), the lack of any relativistic signatures and the very weak BBB (Wu et al. 1983; often interpreted as thermal emission from the disc), this appears to rule out the presence of an inner, ‘classic’ optically thick, geometrically thin accretion disc (Shakura & Sunyaev 1973) envisaged in the unification scheme of AGN (Antonucci 1993). Instead, we suggest that the accretion disc may be truncated at some radius of the order of  $10^3\text{--}10^4 R_{\text{g}}$  ( $\sim 0.01 \text{ pc}$ ) with the inner regions perhaps replaced by a RIAF (Narayan & Yi 1995) consisting of highly ionized, low density ( $n \sim 10^6 \text{ cm}^{-3}$ ), Compton-thin gas covering some significant fraction of  $4\pi \text{ sr}$ . In this scenario, the low accretion rate of the source (0.07 per cent  $L_{\text{Edd}}$ ), perhaps due to a lack of available accreting material, may not allow the infalling material to cool sufficiently in order for a standard thin accretion disc to form. Instead, a stable accretion flow can still occur if the material takes on the form of an optically thin, hot corona, where most of the material is advected across the event horizon as opposed to radiating away the energy it has acquired in moving close to the black hole.

Such a hot, inner flow is expected to comprise a low-density plasma whereby collisional processes dominate over photoionization due to the high temperature. At radii below about  $100 R_{\text{g}}$ , the ion and electron temperatures diverge forming a two-temperature medium with  $T_{\text{e}} \sim 10^9\text{--}10^{10} \text{ K}$  and  $T_{\text{ion}}$  approaching  $10^{12} \text{ K}$  in the innermost regions (Narayan & Yi 1995). The electron temperature  $T_{\text{e}}$  is then expected to fall as  $10^{12} (\text{K})/R$  for  $R > 10^2$ , where  $R$  is in Schwarzschild units. However, further out at  $R \sim 10^3\text{--}10^4 R_{\text{S}}$ , a plasma temperature of a few  $\times 10^8 \text{ K}$  (i.e.  $k_{\text{B}}T \sim 13 \text{ keV}$ , as observed in the collisional APEC model), corresponding to  $R \sim 10^4 R_{\text{S}}$ , would produce emission from both He-like and H-like Fe, as observed. However, while the Fe xxvi emission could plausibly originate in such a plasma, the presence of the Fe xxv forbidden line suggests that the He-like Fe cannot be solely produced in such a collisionally ionized medium. Thus, an alternative picture could instead be that both the Fe xxv and Fe xxvi emission lines originate in photoionized gas, perhaps at the transition region between the RIAF and the cold, outer accretion disc at a radius  $R \sim 10^3\text{--}10^4 R_{\text{g}}$  from the black hole. Alternatively, the Fe xxv/xxvi emission lines may arise from a hybrid of photo- and collisionally-ionized processes.

#### 4.3.2 NGC 7213 as a low/hard state source

The accretion rate of NGC 7213 is much lower than the predicted ‘critical’ value of  $\sim 2$  per cent  $L_{\text{Edd}}$  (Maccarone 2003) whereby the high/soft state in X-ray binaries can be observed. As a result, one interesting possibility is that NGC 7213 is an AGN analogue of the low/hard state observed in Galactic black hole candidates (GBHCs). Long-term monitoring of NGC 7213 with RXTE (Phil Uttley, private communication) shows that the AGN is only slowly variable, indicating a relatively low frequency power spectral density (PSD)

break. This would be consistent with NGC 7213 having a relatively high black hole mass (e.g.  $M_{\text{BH}} = 10^8 M_{\odot}$ ; Nelson & Whittle 1995; Woo & Urry 2002) but a low accretion rate compared to Eddington, consistent with the scaling relations in the timing properties seen between AGN and GBHCs (McHardy et al. 2006). This is further supported by the spectral energy distribution (SED) of NGC 7213 which suggests that this object has interesting radio properties lying between those of radio-loud and radio-quiet quasars (RQQs). Indeed, taking the 5 GHz radio flux and *B*-band flux (host galaxy-subtracted) of Sadler (1984) and Halpern & Filippenko (1984), respectively, and using the equation for radio loudness<sup>6</sup> of Wilkes & Elvis (1986) give a value of  $R_{\text{L}} \sim 2$  suggesting that NGC 7213 is intermediate between radio-quiet AGN and radio-loud AGN such as radio-Galaxies and blazars. However, Panessa et al. (2007) also find that a radio loudness of  $\sim 2$  is not so uncommon in Seyfert galaxies.

The inability to constrain the high-energy cut-off of the X-ray emission (i.e.  $>350 \text{ keV}$ ) could indicate that the continuum emission may be of non-thermal origin with one possibility being that some of the hard X-ray emission that we observe with *Suzaku* originates from the base of a jet.<sup>7</sup> Hameed et al. (2001) imaged NGC 7213 in the optical band and discovered a giant H $\alpha$  filament approximately 19 kpc from the nucleus. They suggest that such a filament could be the signature of neutral gas shock-ionized by the interactions of a jet. A more recent 8.4 GHz Long Baseline Array (LBA) radio study of NGC 7213 (Blank et al. 2005) reports that the source is unresolved on the scale of  $\sim 3 \text{ mas}$  (corresponding to  $\sim 10^4 R_{\text{S}}$  at the distance and black hole mass of NGC 7213), just showing a core, indicating that the jet could be orientated face-on. At lower frequencies, there is also evidence for a large-scale structure ( $\sim 9 \text{ arcmin}$ ; Blank et al. 2005, and reference therein) which could possibly be a signature of the extended radio lobes. Consequently, NGC 7213 is perhaps consistent with the hypothesis of Falcke, Patnaik & Sherwood (1996) whereby the radio-intermediate objects are similar to radio-quiet AGN but with moderate beaming from pc-scale jets orientated face-on to the observer.

#### 4.3.3 The origin of the high-energy continuum

NGC 7213 is not detected to date with the *Fermi* LAT gamma-ray instrument at  $\sim \text{GeV}$  energies (Abdo et al. 2010) where the inverse-Compton emission from the jet would be expected to dominate. The *Fermi* LAT flux limit corresponding to the detection threshold of Abdo et al. (2010) at the Galactic co-ordinates of NGC 7213 and for  $\Gamma = 1.75$  is  $F_{0.1\text{--}100 \text{ GeV}} < 3 \times 10^{-9} \text{ photon cm}^{-2} \text{ s}^{-1}$ . Extrapolating our best-fitting broad-band *Suzaku* model to GeV energies overpredicts the  $\gamma$ -ray flux by a factor of  $\sim \times 100$  returning a predicted photon flux of  $F_{0.1\text{--}100 \text{ GeV}} \sim 3 \times 10^{-7} \text{ photon cm}^{-2} \text{ s}^{-1}$ . This implies that the X-ray continuum does in fact roll over at energies  $>350 \text{ keV}$ .

In order to be consistent with the 0.1–100 GeV flux limit from *Fermi*, we require that the e-folding energy of the power-law component must be  $E_{\text{cut}} < 25 \text{ MeV}$ . This, combined with the lower limit

<sup>6</sup>  $R_{\text{L}} = \log_{10}(F_{5 \text{ GHz}}/F_{\text{B}})$ , where  $F_{5 \text{ GHz}}$  and  $F_{\text{B}}$  are the 5 GHz and *B*-band fluxes, respectively. Typically, a value of  $R_{\text{L}} \geq 1$  signifies a radio-loud object.

<sup>7</sup> Note that the high-energy cut-off was measured with *BeppoSAX* in 2001 to be  $E_{\text{cut}} = 90_{-20}^{+50} \text{ keV}$  (Bianchi et al. 2004). However, we find no evidence for a cut-off energy  $<350 \text{ keV}$  with our combined *Suzaku* XIS, HXD and *Swift* BAT spectra.

on the high-energy cut-off from the combined *Suzaku/Swift* data means that  $350 \text{ keV} < E_{\text{cut}} < 25 \text{ MeV}$ , consistent with the predicted electron temperature of the hot, inner flow (see Section 4.3.1). This suggests that thermal Comptonization is responsible for the X-ray continuum and that any non-thermal contribution from the inverse-Compton component associated with a jet may be negligible in this source.

Furthermore, the high EW of the observed emission lines may also suggest that there is very little dilution of the X-ray continuum by a jet. We note that other radio-loud sources such as the broad-line radio galaxies (BLRGs) 3C 120 and 3C 390.3 do also show fairly strong Fe K line emission with EWs of the order of 50–100 eV. However, in the case of 3C 390.3, Sambruna et al. (2009) argue from the *Suzaku* data and the overall radio- $\gamma$ -ray SED that the jet makes a minimal contribution to the X-ray continuum emission. Likewise, Kataoka, Reeves & Iwasawa (2007) argue a similar case from the *Suzaku* observation of 3C 120 and conclude that the putative jet component does not dilute the Fe K emission. In addition, comparing the ratio of the 1–100 GeV  $\gamma$ -ray flux from *Fermi* to the 2–10 keV X-ray flux for NGC 7213 with that of 3C 111 (the only BLRG detected by *Fermi* to date) and 3C 273, we find that the ratio is higher by a factor of  $> \times 6$  for the two radio-loud AGN. By comparison, like for NGC 7213, none of the X-ray bright type 1 Seyferts appears to have been detected with *Fermi* thus far.

As a further test, we did attempt to model the X-ray continuum with a double power-law component consisting of a hard spectrum to model any possible emission from a jet and a much softer, Seyfert-like spectrum to model the photoionizing nuclear X-ray emission. Statistically speaking, this fit is not required by the data as it only yields an improvement of  $\Delta\chi^2 \sim 2$  for an additional two parameters of interest. Upon fixing the photon index of the softer power law at  $\Gamma = 2$ , we find that the normalization of this component becomes very small with an upper-limit corresponding to just 10 per cent of the normalization of the main power law. So, it seems that a double power-law model is not required by the data and that the X-ray continuum is best represented by a single power-law component.

The photon index of the X-ray continuum has a best-fitting value of  $\Gamma = 1.75 \pm 0.02$ , and therefore has only a slightly flatter spectrum than the typical values usually associated with RQQs and type 1 Seyferts. For example, Reeves & Turner (2000) find a mean value of  $\Gamma = 1.89 \pm 0.05$  from a sample of 27 RQQs observed with the Advanced Satellite for Cosmology and Astrophysics (ASCA) and Nandra & Pounds (1994) find a mean value of  $\Gamma = 1.95$  with a dispersion of  $\sigma = 0.15$  from their sample of Seyfert galaxies observed with *Ginga*. Porquet et al. (2004) also find a mean value of  $\Gamma = 1.90$  with a dispersion of  $\sigma = 0.27$  from a sample of 14 RQQs observed with *XMM-Newton*. The photon index of NGC 7213 is, however, consistent with those found in other low-luminosity AGN such as M81 (Young et al. 2007) and NGC 4579 (Dewangan et al. 2004). Interestingly, the spectrum in NGC 7213 does appear to be somewhat steeper than the predicted photon index of  $\Gamma = 1.4$  from the relation between mass accretion rate and photon index of Papadakis et al. (2009) given its calculated accretion rate of 0.07 per cent  $L_{\text{EDD}}$  (an accretion rate of  $\sim 2$  per cent  $L_{\text{EDD}}$  would be required to obtain  $\Gamma = 1.75$ ). So, it seems that NGC 7213 may not strictly follow the positive correlation between spectral steepness and accretion rate in AGN and X-ray binaries suggested by Shemmer et al. (2006) although the high-energy cut-off of the X-ray continuum (i.e.  $350 \text{ keV} < E_{\text{cut}} < 25 \text{ MeV}$ ) observed here may suggest that the hard X-ray emission that we observe with *Suzaku* and *Swift* could be consistent with a very hot inner flow, compatible with NGC 7213 having a low-mass accretion rate.

## 5 CONCLUSIONS

NGC 7213 is an unusual AGN as it consistently exhibits no evidence for a Compton reflection component unlike in other type 1 Seyferts (Perola et al. 2002; Dadina 2008). The time-averaged continuum emission is well fitted by a single power law of  $\Gamma = 1.75$  and from consideration of the combined *Suzaku* and *Swift* BAT data and the *Fermi* flux limit we constrain the high-energy cut-off to be  $350 \text{ keV} < E_{\text{cut}} < 25 \text{ MeV}$ . The limits on reflection for the neutral and ionized cases from the REFLIONX model are  $R < 0.16$  and  $R < 0.06$ , respectively, suggesting that a significant Compton-thick reflector (e.g. from the inner disc or Compton-thick torus) is absent in this source, consistent with previous findings (e.g. Bianchi et al. 2003). None the less, a significant Fe K complex is observed above 6 keV appearing only in emission. The line from neutral K $\alpha$  dominates (6.39 keV; EW  $\sim 80$  eV) with further contributions from Fe xxv and Fe xxvi Ly $\alpha$  (6.60 and 6.95 keV respectively; also see Starling et al. 2005; Bianchi et al. 2008). Furthermore, in this observation we also find that the Fe xxvi Ly $\alpha$  emission appears to be somewhat resolved in the *Suzaku* spectrum with an FWHM  $\sim 10\,000 \text{ km s}^{-1}$  and that the emission from Fe xxv appears to be consistent with the forbidden transition from helium-like iron at  $\sim 6.64 \text{ keV}$  as opposed to the resonance transition at  $\sim 6.70 \text{ keV}$ .

The neutral K $\alpha$  emission cannot be modelled via reflection off Compton-thick matter. However, an origin in a Compton-thin plasma covering a significant fraction of  $4\pi \text{ sr}$  is feasible with an inferred column density of  $N_{\text{H}} \sim 3\text{--}4 \times 10^{23} \text{ cm}^{-2}$ , again consistent with the findings of previous observations with *Chandra* and *XMM-Newton*. Likewise here, the emission from highly ionized iron can also be modelled with a substantial column ( $N_{\text{H}} \gtrsim 3 \times 10^{23} \text{ cm}^{-2}$ ) of photoionized matter if a location close to the central engine is invoked to explain the inherent broadening and the high ionization state. Given the lack of either neutral or ionized reflection coupled with the apparent absence of any relativistic signature in the spectrum, it appears that an inner, optically thick accretion disc may be absent in this source. Instead, the accretion disc in NGC 7213 is most likely truncated at some radius with the inner regions perhaps replaced by an advective accretion flow (e.g. RIAF; Narayan & Yi 1995). The Fe xxv/xxvi emission could then be the ionized signature of such a hot, optically thin plasma originating in material a few  $\times 10^3 R_{\text{g}}$  from the central X-ray source.

## ACKNOWLEDGMENTS

This research has made use of the NASA Astronomical Data System (ADS), the NASA Extragalactic Database (NED) and data obtained from the *Suzaku* satellite, a collaborative mission between the space agencies of Japan (JAXA) and the USA (NASA). We wish to thank our anonymous referee for their useful comments and thorough review of the draft. Valentina Braitto would also like to acknowledge support from the UK STFC research council.

## REFERENCES

- Abdo A. A. et al., 2010, ApJ, 715, 429
- Anders E., Ebihara M., 1982, Geochim. Cosmochim. Acta, 46, 2363
- Anders E., Grevesse N., 1989, Geochim. Cosmochim. Acta, 53, 197
- Antonucci R., 1993, ARA&A, 31, 473
- Arnaud K. A., 1996, in Jacoby G. H., Barnes J., eds, ASP Conf. Ser. Vol. 101, Astronomical Data Analysis Software and Systems V, Astron. Soc. Pac., San Francisco, p. 17
- Bautista M. A., Kallman T. R., 2000, ApJ, 544, 581
- Bianchi S., Matt G., 2002, A&A, 387, 76

- Bianchi S., Matt G., Balestra I., Perola G. C., 2003, *A&A*, 407, L21
- Bianchi S., Matt G., Balestra I., Guainazzi M., Perola G. C., 2004, *A&A*, 422, 65
- Bianchi S., Matt G., Nicastro F., Porquet D., Dubau J., 2005, *MNRAS*, 357, 599
- Bianchi S., La Franca F., Matt G., Guainazzi M., Jiménez-Bailón E., Longinotti A. L., Nicastro F., Pentericci L., 2008, *MNRAS*, 389, L52
- Blank D. L., Harnett J. I., Jones P. A., 2005, *MNRAS*, 356, 734
- Boldt E., 1987, *Phys. Rep.*, 146, 215
- Brinkman A. C., Kaastra J. S., van der Meer R. L. J., Kinkhabwala A., Behar E., Kahn S. M., Paerels F. B. S., Sako M., 2002, *A&A*, 396, 761
- Churazov E., Sunyaev R., Revnivtsev M., 2007, *A&A*, 467, 529
- Dadina M., 2008, *A&A*, 485, 417
- Dewangan G. C., Griffiths R. E., Di Matteo T., Schurch N. J., 2004, *ApJ*, 607, 788
- Dickey J. M., Lockman F. J., 1990, *ARA&A*, 28, 215
- Fabian A. C., Rees M. J., Stella L., White N. E., 1989, *MNRAS*, 238, 729
- Falcke H., Patnaik A. R., Sherwood W., 1996, *ApJ*, 473, L13
- Filippenko A. V., Halpern J. P., 1984, *ApJ*, 285, 458
- Fukazawa Y. et al., 2009, *PASJ*, 61, 17
- George I. M., Fabian A. C., 1991, *MNRAS*, 249, 352
- Grevesse N., Noels A., Sauval A. J., 1996, in Holt S. S., Sonneborn G. (eds), *ASP Conf. Ser. Vol. 99, October Astrophysics Conference*. Astron. Soc. Pac., San Francisco, p. 117
- Gruber D. E., Matteson J. L., Peterson L. E., Jung G. V., 1999, *ApJ*, 520, 124
- Halpern J. P., Filippenko A. V., 1984, *ApJ*, 285, 475
- Hameed S., Blank D. L., Young L. M., Devereux N., 2001, *ApJ*, 546, 97
- Ho L. C., 1999, *ApJ*, 516, 672
- Ishida M., Suzuki K., Someya K., 2007, *PJX-ISAS-SUZAKU-MEMO-2007-11*, 1
- Ishisaki Y. et al., 2007, *PASJ*, 59, 113
- Kaastra J. S., Mewe R., 1993, *A&AS*, 97, 443
- Kalberla P. M. W., Burton W. B., Hartmann D., Arnal E. M., Bajaja E., Morras R., Pöppel W. G. L., 2005, *A&A*, 440, 775
- Kallman T. R., McCray R., 1982, *ApJ*, 50, 263
- Kaspi S. et al., 2001, *ApJ*, 554, 216
- Kataoka J., Reeves J. N., Iwasawa K., 2007, *PASJ*, 59, 279
- Kinkhabwala A. et al., 2002, *ApJ*, 575, 732
- Kokubun M. et al., 2007, *PASJ*, 59, 53
- Koyama K. et al., 2007, *PASJ*, 59, 23
- Maccarone T. J., 2003, *A&A*, 409, 697
- Magdziarz P., Zdziarski A. A., 1995, *MNRAS*, 273, 837
- Matt G., Perola G. C., Pirlo L., 1991, *A&A*, 247, 25
- McHardy I. M., Koerding E., Knigge C., Uttley P., Fender R. P., 2006, *Nat*, 444, 730
- Mitsuda K. et al., 2007, *PASJ*, 59, 1
- Morrison R., McCammon D., 1983, *ApJ*, 270, 119
- Mould J. et al., 2000, *ApJ*, 529, 786
- Murphy K. D., Yaqoob T., 2009, *MNRAS*, 397, 1549
- Nandra K., Pounds K. A., 1994, *MNRAS*, 268, 405
- Narayan R., Yi I., 1995, *ApJ*, 452, 710
- Nelson C. H., Whittle M., 1995, *ApJS*, 99, 67
- Netzer H., Laor A., 1993, *ApJ*, 404, 51
- Padovani P., Rafanelli P., 1988, *A&A*, 205, 53
- Page M. J., 2001, *MNRAS*, 328, 925
- Page M. J., Breeveld A. A., Soria R., Wu K., Branduardi-Raymont G., Mason K. O., Starling R. L. C., Zane S., 2003, *A&A*, 400, 145
- Panessa F., Barcons X., Bassani L., Cappi M., Carrera F. J., Ho L. C., Pellegrini S., 2007, *A&A*, 467, 519
- Papadakis I. E., Sobolewska M., Arevalo P., Markowitz A., McHardy I. M., Miller L., Reeves J. N., Turner T. J., 2009, *A&A*, 494, 905
- Perola G. C., Matt G., Cappi M., Fiore F., Guainazzi M., Maraschi L., Petrucci P. O., Piro L., 2002, *A&A*, 389, 802
- Porquet D., Dubau J., 2000, *A&AS*, 143, 495
- Porquet D., Reeves J. N., O'Brien P., Brinkmann W., 2004, *A&A*, 422, 85
- Pounds K. A., Page K. L., 2005, *MNRAS*, 360, 1123
- Reeves J. N., Turner T. J., 2000, *MNRAS*, 316, 234
- Ross R. R., Fabian A. C., 2005, *MNRAS*, 358, 211
- Sadler E. M., 1984, *AJ*, 89, 53
- Sambruna R. M. et al., 2009, *ApJ*, 700, 1473
- Schurch N. J., Warwick R. S., 2002, *MNRAS*, 334, 811
- Shakura N. I., Sunyaev R. A., 1973, *A&A*, 24, 337
- Shemmer O., Brandt W. N., Netzer H., Maiolino R., Kaspi S., 2006, *ApJ*, 646, 29
- Smith R. K., Brickhouse N. S., Liedahl D. A., Raymond J. C., 2001, *ApJ*, 556, L91
- Starling R. L. C., Page M. J., Branduardi-Raymont G., Breeveld A. A., Soria R., Wu K., 2005, *MNRAS*, 356, 727
- Takahashi T. et al., 2007, *PASJ*, 59, 35
- Tueller J. et al., 2010, *ApJS*, 186, 378
- Verner D. A., Ferland G. J., Korista K. T., Yakovlev D. G., 1996, *ApJ*, 465, 487
- Wandel A., 1999, *ApJ*, 527, 657
- Wilkes B. J., Elvis M., 1986, *BAAS*, 18, 925
- Woo J.-H., Urry C. M., 2002, *ApJ*, 579, 530
- Wu C.-C., Boggess A., Gull T. R., 1983, *ApJ*, 266, 28
- Yaqoob T., Murphy K. D., Miller L., Turner T. J., 2010, *MNRAS*, 401, 411
- Young A. J., Nowak M. A., Markoff S., Marshall H. L., Canizares C. R., 2007, *ApJ*, 669, 830

This paper has been typeset from a  $\text{\TeX}/\text{\LaTeX}$  file prepared by the author.